www.nature.com/aps

Acta Pharmacologica Sinica

ARTICLE

Paris saponin VII, a Hippo pathway activator, induces autophagy and exhibits therapeutic potential against human breast cancer cells

Yu-chen Xiang[1,2], Peng Peng[1,3], Xue-wen Liu[1,4], Xin Jin[1,2], Jie Shen[1,2], Te Zhang[2,4], Liang Zhang[1,3], Fang Wan[1,2], Yu-liang Ren[1,2], Qing-qing Yu[3,4], Hu-zi Zhao[1,3,4], Yuan Si[1,3,4] and Ying Liu[1,2,3,4]

Dysregulation of the Hippo signaling pathway seen in many types of cancer is usually associated with a poor prognosis. Paris saponin VII (PSVII) is a steroid saponin isolated from traditional Chinese herbs with therapeutic action against various human cancers. In this study we investigated the effects of PSVII on human breast cancer (BC) cells and its anticancer mechanisms. We showed that PSVII concentration-dependently inhibited the proliferation of MDA-MB-231, MDA-MB-436 and MCF-7 BC cell lines with IC_{50} values of 3.16, 3.45, and 2.86 μM, respectively, and suppressed their colony formation. PSVII (1.2–1.8 μM) induced caspase-dependent apoptosis in the BC cell lines. PSVII treatment also induced autophagy and promoted autophagic flux in the BC cell lines. PSVII treatment decreased the expression and nuclear translocation of Yes-associated protein (YAP), a downstream transcriptional effector in the Hippo signaling pathway; overexpression of YAP markedly attenuated PSVII-induced autophagy. PSVII-induced, YAP-mediated autophagy was associated with increased active form of LATS1, an upstream effector of YAP. The activation of LATS1 was involved the participation of multiple proteins (including MST2, MOB1, and LATS1 itself) in an MST2-dependent sequential activation cascade. We further revealed that PSVII promoted the binding of LATS1 with MST2 and MOB1, and activated LATS1 in the BC cell lines. Molecular docking showed that PSVII directly bound to the MST2-MOB1-LATS1 ternary complex. Microscale thermophoresis analysis and drug affinity responsive targeting stability assay confirmed the high affinity between PSVII and the MST2-MOB1-LATS1 ternary complex. In mice bearing MDA-MB-231 cell xenograft, administration of PSVII (1.5 mg/kg, ip, 4 times/week, for 4 weeks) significantly suppressed the tumor growth with increased pLATS1, LC3-II and Beclin 1 levels and decreased YAP, p62 and Ki67 levels in the tumor tissue. Overall, this study demonstrates that PSVII is a novel and direct Hippo activator that has great potential in the treatment of BC.

Keywords: anti cancer drug pharmacology; autophagy; Chinese traditional medicine; molecular docking; Breast cancer; Hippo pathway activator

Acta Pharmacologica Sinica (2022) 43:1568–1580; https://doi.org/10.1038/s41401-021-00755-9

INTRODUCTION

Breast cancer (BC) is one of most common malignant tumors worldwide and seriously threatens women's health. In 2020, BC surpassed lung cancer as the most commonly diagnosed cancer, with an estimated 2.3 million new cases (11.7%) and 684,996 deaths (6.9%) estimated worldwide [1]. In addition, the incidence of this disease ranks fourth among different types of tumors in China [2]. The treatments for BC mainly include surgery, chemotherapy, radiotherapy, and hormonotherapy. However, the long-term clinical prognosis and patient survival are still dissatisfactory [3]. Therefore, the investigation of novel anticancer agents for BC is expected to lead to improved diagnosis and treatment.

Autophagy, characterized by the formation of double-membrane autophagosomes, is a highly conserved process that maintains intracellular metabolism and homeostasis in all eukaryotic cells [4]. In this process, proteins and organelles are first phagocytized by autophagosomes, then delivered to lysosomes and finally degraded and recycled. Starvation, hypoxia, infection, a high reactive oxygen species content, and endoplasmic reticulum stress can all trigger autophagy [5]. Autophagy is closely associated with metabolic diseases, neurodegeneration, cancer, immunity, heart disease, and especially cancer. Autophagy is a "double-edged sword" in cancer [6]. On the one hand, autophagy activation can promote the survival of cancer cells, which is called protective autophagy. On the other hand, autophagy activation can lead to the death of cancer cells, which is referred to as cytotoxic/nonprotective autophagy [7]. Despite this dichotomy, cytotoxic autophagy clearly plays an important role in anticancer research. Several approved and/or experimental drugs and natural compounds (such as metformin, curcumin, and quercetin) induce autophagy in different types of

[1]Laboratory of Molecular Target Therapy of Cancer, Institute of Basic Medical Sciences, Hubei University of Medicine, Shiyan 442000, China; [2]Hubei Key Laboratory of Wudang Local Chinese Medicine Research, Hubei University of Medicine, Shiyan 442000, China; [3]Hubei Key Laboratory of Embryonic Stem Cell Research, Hubei University of Medicine, Shiyan 442000, China and [4]Laboratory of Molecular Target Therapy of Cancer, Biomedical Research Institute, Hubei University of Medicine, Shiyan 442000, China
Correspondence: Yuan Si (siyuan138@126.com) or Ying Liu (ying_liu1002@163.com)
These authors contributed equally: Yu-chen Xiang, Peng Peng

Received: 22 April 2021 Accepted: 2 August 2021
Published online: 14 September 2021

cancer [8–10]. Therefore, activating autophagy is considered an effective strategy for anti-cancer drug discovery and treatment.

The highly conserved Hippo signaling pathway plays important roles in monitoring organ size, tissue homeostasis, cell proliferation and death, and stem cell self-renewal [11]. The Hippo pathway consists of a core serine–threonine kinase cascade and a transcriptional module. The upstream mammalian STE-20-like protein kinase 1/2 (MST1/2) phosphorylates and activates the downstream large tumor-suppressor kinase 1/2 (LATS1/2). The adapter protein MOB kinase activator 1 (MOB1) is involved in the phosphorylation of LATS1/2. Phosphorylated LATS1/2 then phosphorylates and inactivates the transcriptional coactivator Yes-associated protein (YAP) and transcriptional coactivator with the PDZ-binding motif (TAZ) to retain them in the cytoplasm and prevent their nuclear import for transcriptional activation. Dephosphorylated YAP/TAZ translocates to the nucleus and associates with transcription factors such as TEA domain (TEAD) family members to accelerate growth- and invasion-related gene expression [12, 13]. The Hippo pathway is dysregulated in a variety of human cancers, including BC, colorectal cancer, lung cancer, ovarian cancer, gastric cancer, and liver cancer and it is usually associated with a poor prognosis [14–16]. Recently, Wu et al. reviewed that each component of the core Hippo pathway is involved in the tumorigenesis and metastasis of BC and described drugs targeting the Hippo pathway for BC treatment [17]. However, research and drug discovery targeting the Hippo pathway in BC is still rare, and there is an urgent need to discover new activators for BC treatment.

Paris polyphylla and *Trillium tschonoskii* Maxim (TTM) are characteristic medicinal plants that are widely distributed in the Wudang Mountains and Shennongjia National Natural Reserve of China. They both grow in forests at an altitude of 1600–3200 meters in damp valleys on hillsides or under roadside rocks. Both of these plants belong to the lily family, and their rhizomes are used as traditional Chinese medicine to treat several diseases [18–21]. Paris saponin VII (PSVII, Fig. 1), also called Dioscinin, Polyphyllin VII and Chonglou saponin VII, is a steroidal saponin isolated from the rhizome of *Paris polyphylla* and TTM [21]. PSVII has been reported to have therapeutic effects in several types of cancer [22–25]. However, its specific targets and mechanisms are still unclear. This article aims to explore the antitumor effect and potential mechanisms of PSVII in BC.

MATERIALS AND METHODS

Reagents

PSVII with a purity of up to 95% was purchased from Shanghai YuanYe BioTechnology Co., Ltd. (Shanghai, China). PSVII was dissolved in dimethylsulfoxide (DMSO, Sigma-Aldrich, Merck KGaA, Darmstadt, Germany) at a stock solution of 50 mM and stored at −20 °C.

Cell culture

Human BC cell lines MCF-7, MDA-MB-231, MDA-MB-436, BT474, SKBR3, and non-tumorigenic MCF-10A human mammary epithelial cells (MCF-10A) were obtained from American Type Culture Collection (ATCC, Manassas, VA, USA). MCF-7, BT474, SKBR3, and MDA-MB-231 cells were cultured in Dulbecco's modified Eagle's medium (DMEM, Gibco; Thermo Fisher Scientific, Inc., Waltham, MA, USA). MDA-MB-436 cells were cultured in Leibovitz's -15 (L-15) medium (Gibco, Thermo Fisher Scientific, Inc.). DMEM and L-15 medium were supplemented with 10% fetal bovine serum (FBS, HyClone, Logan, UT, USA), 100 U/mL penicillin, and 100 μg/mL streptomycin (both from Gibco, Thermo Fisher Scientific, Inc.) and cultured in a humidified atmosphere with 5% CO_2 at 37 °C. MCF-10A cells were maintained in DMEM/F12 medium containing 5% horse serum (HS), insulin (10 mg/mL), epidermal growth factor (EGF, 20 ng/mL), choleratoxin (100 mg/mL), hydrocortisone (0.5 mg/mL), penicillin (50 U/mL), and streptomycin (50 U/mL), and incubated in a humidified atmosphere with CO_2 at 37 °C.

Cytotoxic assay, cell viability

Cells were seeded onto a 96-well plate, pre-cultured for 24 h, and then treated with PSVII for 24 h. Cell cytotoxicity was investigated by a CCK-8 assay. The absorbance was determined at 450 nm by an automated microplate reader (Bio-Tek, VT, USA), and the inhibition rate was calculated as follows: inhibition rate (%) = (average A_{450} of the control group − average A_{450} of the experimental group)/(average A_{450} of the control group − average A_{450} of the blank group) × 100%. Cell viability was determined by trypan blue dye exclusion [26].

Soft agar colony formation assay

Cells were suspended in 1 mL of DMEM or L-15 containing 0.3% low-melting-point agarose (Amresco, Cleveland, Oh, USA) and 10% FBS, and plated on a bottom layer containing 0.6% agarose and 10% FBS in six-well plate in triplicate. After 2 weeks, plates were stained with 0.2% gentian violet and the colonies were counted under light microscope (IX70, Olympus Corporation, Tokyo, Japan).

Flow cytometry assays

Cells were seeded in six-well plate and incubated with PSVII for 24 h. Cell apoptosis was evaluated by AV/PI detection using an AV-

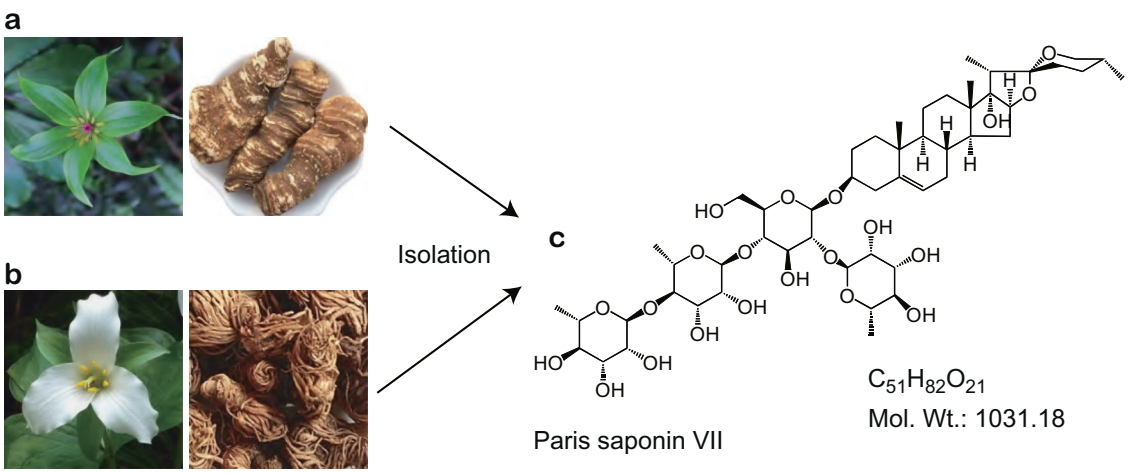

Fig. 1 Chemical structure of PSVII. a Plant and root of *Paris polyphylla*. **b** Plant and root of *Trillium tschonoskii* Maxim. **c** Structure of Paris saponin VII.

FITC kit (BD Biosciences, San Jose, CA, USA), flow cytometry was performed using a BD FACScanto II flow cytometer (Becton Dickinson, San Jose, CA), and at least 10,000 cells were counted for each sample [27].

DAPI staining

To observe nuclear morphology, cells treated under the indicated conditions were fixed in 4% paraformaldehyde, incubated with 4′,6-diamidino-2-phenylindole (DAPI; Sigma Chemical Co.), and then analyzed using a fluorescence microscope (Olympus, Japan).

Western blot analysis

Cells were harvested and lysed with RIPA buffer to extract total protein. Total protein was loaded on 8%–12% SDS-PAGE. Subsequently, the gel was electrophoretically transferred to a PVDF membrane (Millipore, Kenilworth, NJ, USA). After blocked with 5% nonfat dry milk for 1 h at room temperature, the membrane was incubated with the primary antibody overnight at 4 °C and washed three times with Tris buffered saline containing 0.5% Tween-20. The following primary antibodies were used: anti-caspase-3 (1: 1000; catalog no. 9664), anti-caspase-8 (1: 1000; catalog no. 9748), anti-PARP (1: 1000; catalog no. 9548), anti-LC3 (1: 1000; catalog no. 12741), anti-phospho-YAP (S127) (1: 1000; catalog no. 4911), anti-LATS1 (1: 1000; catalog no. 3477), anti-phospho-LATS1 (T1079) (1: 1000; catalog no. 8654), anti-MOB1 (1: 1000; catalog no. 3477), anti-phospho-MOB1 (T35) (1: 1000; catalog no. 8699), anti-phospho-MST2 (T180) (1: 1000; catalog no. 49332) (Cell Signaling Technology, Inc., Danvers, MA, USA), anti-YAP (1: 500; catalog no. sc-101199), anti-Cyr61 (1: 500; catalog no. sc-374129) (Santa Cruz Biotechnology, Santa Cruz, CA, USA), anti-MST2 (1: 1000; catalog no. Ab52641; Abcam), anti-p62 (1: 1000; catalog no. P0067; Sigma), and anti-GAPDH (1: 5000; catalog no. M20006; Abmart, Shanghai, China). The blots were then washed, and incubated with a horseradish peroxidase (HRP)-conjugated secondary antibody (1: 10000; catalog no. E030120-01(rabbit) and E030110-01(mouse); EarthOx, LLC, San Francisco, CA, USA) at room temperature for 1.5 h. Detection was performed using a Super-Signal® West Pico Trial kit (catalog no. QA210131; Pierce Biotechnology, Inc., Rockford, IL, USA) [28].

Real-time quantitative PCR (qPCR)

Total RNA was extracted from cells using Trizol reagent (Invitrogen; Thermo Fisher Scientifc, Inc., Waltham, MA, USA) according to the manufacturer's protocol. Real-time quantitative PCR (qPCR) analysis was performed with 2 μg of total RNA and ReverTra Ace qPCR RT Kit (Toyobo Co., Ltd. Life Science Department, Osaka Japan). We mixed 2 μg RNA, 4 μL 5 × RT Buffer, 1 μL RT Enzyme Mix, 1 μL Primer Mix, and Nuclease-free Water up to 20 μL volume. The reverse transcription step was as follows: 37 °C for 15 min; 98 °C for 5 min, then stored at −20 °C. qPCR was performed in an ABI StepOnePlus™ Real-Time PCR System (ABI; Thermo Fisher Scientific, Inc., Waltham, MA, USA) using SYBR® Green Real-time PCR Master Mix (Toyobo Co., Ltd. Life Science Department, Osaka Japan). We mixed SYBR Green PCR Master Mix 10 μL, forward and reverse primers 200 nM, cDNA template 100 ng, and ddH_2O up to 20 μL volume. PCR conditions consisted of the following: 95 °C for 3 min for denaturation; 95 °C for 15 s for annealing; and 60 °C for 1 min for extension, for 40 cycles. The threshold cycle for each sample was selected from the linear range and converted to a starting quantity by interpolation from a standard curve generated on the same plate for each set of primers Table 1. The *CTGF* and *Cyr61* mRNA levels were normalized for each well to the *GAPDH* mRNA levels using the $2^{-\Delta\Delta Ct}$ method. Each experiment was repeated three times.

Autophagy assays

The cells were transfected with pQCXIP-GFP-LC3 or pmRFP-GFP-LC3 plasmid using the Lipofectamine 3000 (Invitrogen; Thermo Fisher Scientific, Inc.) according to the recommended protocol by the manufacturer and then treated with PSVII for 24 h. The cells were fixed in 4% paraformaldehyde. The percentage of cells with fluorescent dots representing GFP-LC3 translocation was counted. For visualization of cell nucleus, DAPI was used. Sections were observed using an Olympus laser scanning confocal microscope with imaging software (Olympus Fluoview FV-1000, Tokyo, Japan) [29].

Table 1. Primer sequences for qPCR.

Gene	Primer sequence (5′-3′)
CTGF	F: CCAATGACAACGCCTCCTG
	R: TGGTGCAGCCAGAAAGCTC
Cyr61	F: AGCCTCGCATCCTATACAACC
	R: TTCTTTCACAAGGCGGCACTC
GAPDH	F: GGTCTCCTCTGACTTCAACA
	R: GTGAGGGTCTCTCTCTTCCT

F forward, *R* reverse.

Immunoprecipitation

Cells were cotransfected with HA-LATS1/Flag-MST2, HA-LATS1/Myc-MOB1, or Flag-MST2/Myc-MOB1 vectors. At 24 h post transfection, cells were treated with PSVII for 24 h and then lysed with lysis buffer (50 mM HEPES at pH 7.5, 150 mM NaCl, 1 mM EDTA, 1% NP-40, 10 mM pyrophosphoate, 10 mM glycerophosphate, 50 mM NaF, 1.5 mM Na_3VO_4, protease inhibitor cocktail, 1 mM DTT, 1 mM PMSF) and immunoprecipitated with anti-HA, anti-Flag, or anti-Myc antibodies. The precipitated proteins were lysed with SDS loading buffer and analyzed by Western blot.

Molecular docking

For the complex of MST2, MOB1, and LATS1 protein, we first tried to use modeling and ZDOCK docking to obtain the three complexes. After modeling, the random coils of the MST2 loop structure were too flexible, resulting in unsatisfactory protein-protein docking conformation. According to the PDB library, 5BRM and 5BRK are respectively MOB1-MST2 binding structure and MOB1-LATS1 binding structure. By using the Align mode in pymol software, we take the chain A (MOB1), chain G (MST2) of 5BRM, and chain B (LATS1) of 5BRK, and finally get the MST2-MOB1-LATS1 complex. The core of phospho-MOB1(pMOB1^{core}) is green, the MOB1 binding domain of LATS1 (LATS1^{MBD}) is cyan, the MOB1 binding motif of phospho-MST2 (pMST2^{MBM}) is magenta, and the PSVII is gold. Ligand docking studies were performed with Autodock 4. The chemical structure of PSVII was shown in Fig. 1. Docking was performed with the docking box whose size is large enough to include the binding sites.

Microscale thermophoresis assay

PSVII at different concentrations was mixed with labelled Homo LATS1, MOB1, or MST2 (Abcam, Cambridge, UK) and incubated for 30 min at room temperature. The specimens were loaded and measured on a Monolith NT.115 instrument (Nano Temper Technologies, München, Germany). The dissociation constant (K_d) values were fitted by the NT Analysis software (Nano Temper Technologies, München, Germany) [30].

Drug affinity responsive target stability assay

Cells were harvested and lysed with cell lysis buffer (Thermo Fisher Scientific, Inc., Waltham, MA, USA) to extract total protein. Total protein was treated with different concentrations of PSVII and incubated with pronase (Sigma) at 37 °C for 30 min. The extent of hydrolyzation of each specimen was measured by Western blot [31].

Xenograft experiments

Female nude immunodeficient mice (*nu/nu*), 5–7 weeks old, were purchased from Hunan SJA Laboratory Animal Co., Ltd. (Changsha, China), and maintained and monitored in a specific pathogen-free environment. The mice were injected subcutaneously with 6×10^6 MDA-MB-231 cells in 100 μL DMEM into the right flank. Treatments were started when the tumors reached a palpable size. Mice were then randomly divided into two groups: vehicle group (0.8% DMSO, 12% cremophor, and 8% ethanol in normal saline; $n = 8$) and PSVII-treated group (intraperitoneal injection of 1.5 mg/kg PSVII; $n = 8$). The mice were treated four times per week for a total of 30 days. Caliper measurements of the longest perpendicular tumor diameters were performed twice a week to estimate the tumor volume, using the following formula: $4\pi/3 \times (\text{width}/2)^2 \times (\text{length}/2)$, representing the three-dimensional volume of an ellipse. Animals were sacrificed when tumors reached 1.5 cm or if the mice appeared moribund to prevent unnecessary morbidity to the mice. At the time of the animals' death, subcutaneous tumors were excised for Western blot and fixed in 10% formalin and then, embedded in paraffin for H&E staining and immunohistochemistry.

Pharmacokinetic study

Eight Sprague–Dawley (SD) rats (220–250 g, female) were bought from Hunan SJA Laboratory Animal Co., Ltd. (Changsha, China), and maintained and monitored in a specific pathogen-free environment. They were fasted overnight before the experiments. All rat studies were conducted according to protocols approved by the Animal Ethics Committee of Hubei University of Medicine. Four rats were administered with PSVII (1 mg/kg) by intravenous injection, and the other four rats were inoculated with PSVII (10 mg/kg) by intragastric injection. Blood samples of 100–200 μL was collected from the orbit at the time points indicated. The plasma concentrations of PSVII were determined by LC-MS/MS. The pharmacokinetic parameters were obtained from the pharmacokinetic software DAS 2.0 (Drug and Statistics Version 2.0).

Statistical analysis

All statistical analyses were conducted using GraphPad Prism 8 (GraphPad Software, Inc., La Jolla, CA, USA) and SPSS 22.0 software for Windows (IBM Corp., Armonk, NY, USA). Results from three independent experiments were presented as the mean ± standard deviation unless otherwise noted. Statistically significant values were compared using Student's *t* test of unpaired data or one-way analysis of variance and Bonferroni's *post hoc* test. $P < 0.05$ was used to indicate a statistically significant difference.

RESULTS

PSVII inhibits the proliferation of BC cells

We tested the effects of PSVII on BC cells and normal MCF-10A human mammary epithelial cells and found that the MCF-10A cells had reduced sensitivity to PSVII, with an IC_{50} value of 8.51 μM. IC_{50} values showed that MDA-MB-231, MDA-MB-436, and MCF-7 cells were more sensitive to PSVII, therefore these three cell lines were subsequently selected for follow-up mechanistic investigation (Table 2). The IC_{50} values of PSVII in MDA-MB-231, MDA-MB-436, and MCF-7 cells were 3.16 μM, 3.45 μM, and 2.86 μM, respectively, at 24 h (Fig. 2a). Trypan blue exclusion assays showed that PSVII reduced the number of viable MDA-MB-231, MDA-MB-436, and MCF-7 cells (Fig. 2b) in a dose- and time-dependent manner. Colony formation assays showed that PSVII markedly inhibited the clonogenic ability of MDA-MB-231, MDA-MB-436, and MCF-7 cells (Fig. 2c). These results suggested that PSVII inhibited anchorage-dependent (cell viability) and anchorage-independent (colony formation) growth of BC cells. In the remainder of the study, the dose of PSVII that was selected for inhibition was <30% to ensure cellular integrity.

PSVII induces caspase-dependent apoptosis of BC cells

Apoptosis was further analyzed in MDA-MB-231, MDA-MB-436, and MCF-7 cells. Annexin V/PI staining and flow cytometry assays confirmed that PSVII treatment induced the apoptosis of MDA-MB-231, MDA-MB-436, and MCF-7 cells (Fig. 3a). DAPI staining further showed that PSVII induced chromatin condensation and fragmentation in MDA-MB-231, MDA-MB-436, and MCF-7 cells, which showed typical nuclear morphological changes that are indicative of apoptosis (Fig. 3b). Next, Western blot analysis revealed that PSVII induced a significant decrease in the precursor form of caspase-3 (pro-casp3) and caspase-8 (pro-casp8) and induced cleavage of poly (ADP-ribose) polymerase (PARP) in MDA-MB-231, MDA-MB-436, and MCF-7 cells (Fig. 3c). These results indicate that PSVII induces caspase-dependent apoptosis of BC cells.

PSVII induces autophagosome formation and promotes autophagic flux in BC cells

Autophagy is a biological survival mechanism that is activated in cells during stress. The formation of autophagosomes requires the recruitment of microtubule-associated protein 1A/1B-light chain 3 (LC3-I) protein, which is site-specifically hydrolyzed to conjugate with phosphatidylethanolamine and is converted into the lipidated LC3-II form [32, 33]. Thus, the amount of LC3-II positively correlates with the number of autophagosomes. Western blot analysis showed that PSVII treatment resulted in a dose- and time-dependent accumulation of LC3-II in MDA-MB-231, MDA-MB-436, and MCF-7 cells (Fig. 4a–b). To determine whether PSVII induces the formation of autophagosomes, an exogenous GFP-LC3 plasmid was transfected into MDA-MB-231, MDA-MB-436, and MCF-7 cells, which were then treated with PSVII. Autophagosome accumulation was detected with a fluorescence microscope. The results showed that the control cells of MDA-MB-231, MDA-MB-436, and MCF-7 cells displayed diffuse staining, while upon PSVII treatment, the cells exhibited a speckled fluorescence staining pattern (Fig. 4c), indicating the redistribution of LC3 to autophagosomes. These results suggested that PSVII treatment induced autophagy. We hypothesized that the cytotoxicity of PSVII is related to autophagy induction in BC cells. PSVII and the autophagy inhibitor 3-MA were combined and used to treat BC cells. Western blot analysis suggested that 3-MA antagonized the PSVII-induced increase in LC3-II (Fig. 4d). Furthermore, we showed that 3-MA significantly reversed the cell proliferation that was inhibited by PSVII (Fig. 4e). These results suggested that PSVII may inhibit the proliferation of BC cells by activating autophagy.

The increase in the number of autophagosomes is either due to their increased synthesis or to a block in their transport to lysosomes [34]. Next, autophagic flux was detected to determine the cause of autophagosome accumulation. Fig. 4f showed that PSVII decreased the expression of p62 in BC cells, which is a substrate of autophagy transports to lysosomes for degradation, suggesting that autophagic flux is not blocked. Next, the pmRFP-GFP-LC3 plasmid was transfected into BC cells, which were then treated with PSVII. The distribution of the pmRFP-GFP-LC3 fusion protein was analyzed (Fig. 4g–h). The results showed that PSVII caused notable emission of red fluorescence, indicating autophagolysosome formation, and a moderate increase in yellow fluorescence emission, indicating autophagosome formation, suggesting the fusion of autophagosomes with lysosomes. Furthermore, lysosomal pH was examined using acridine orange (AO) staining, as lysosomes are characterized by an acidic environment. Upon PSVII treatment, the amount of red fluorescence emitted was greatly increased, suggesting that PSVII reduced the pH in the acidic compartments (Fig. 4i). Taken together, these results suggested that PSVII induced autophagosome formation and increased autophagic flux in BC cells.

Table 2. IC_{50}s of PSVII on BC cell lines.

Cell lines	MCF-10A	SKBR3	BT474	MDA-MB-436	MDA-MB-231	MCF-7
IC_{50} (μM)	7.62 ± 0.51	5.19 ± 0.64	4.04 ± 0.36	3.45 ± 0.48	3.16 ± 0.23	2.86 ± 0.26

The cells were treated with PSVII at various concentrations for 24 h, the cell cytotoxicity was analyzed by CCK-8 assay, and the IC_{50} was calculated using CalcuSyn (version 2.1). Values shown are means plus or minus SD of quadruplicate determinations.

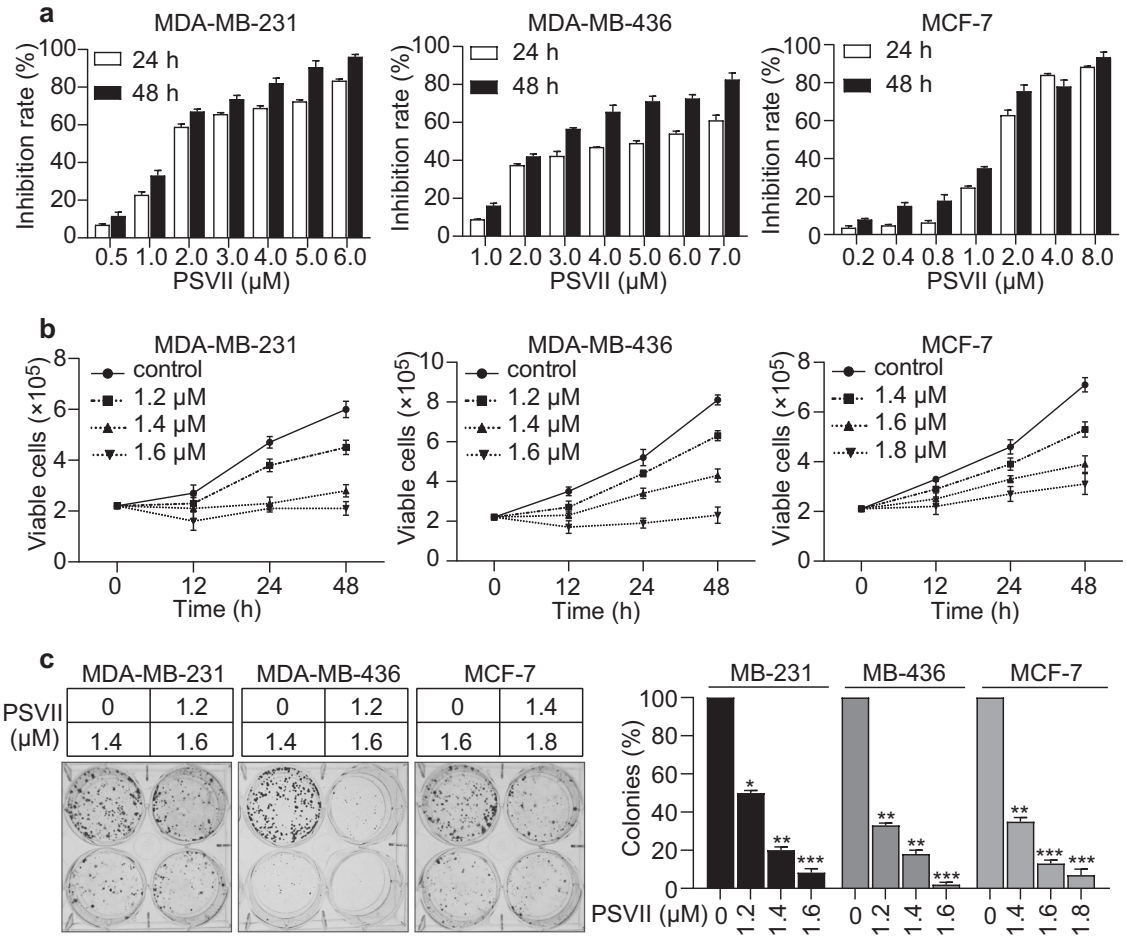

Fig. 2 Effect of PSVII in BC cells. a The inhibitory effects of PSVII on MDA-MB-231, MDA-MB-436, and MCF-7 cells were analyzed by CCK-8 assay. **b** The inhibitory effects of PSVII on the viability of MDA-MB-231, MDA-MB-436, and MCF-7 cells were assayed by trypan blue exclusion assay. **c** Colony formation assays of MDA-MB-231, MDA-MB-436, and MCF-7 cells treated with PSVII at the indicated concentrations. $^{*}P < 0.05$, $^{**}P < 0.01$, $^{***}P < 0.001$. The data are representative of at least three experiments.

PSVII induces autophagy via Hippo signaling pathway activation in BC cells

Recently, the Hippo-YAP axis has been extensively referred to as the driver of the pathophysiological processes that mediate autophagy. The expression and phosphorylation of YAP was detected by Western blot analysis. As shown in Fig. 5a, the phosphorylation of YAP at Ser127 (pYAP) was upregulated and the expression of YAP was downregulated in MDA-MB-231, MDA-MB-436, and MCF-7 cells following treatment with PSVII. Further investigation of the expression of YAP downstream target genes (*CTGF* and *Cyr61*) showed that PSVII downregulated the mRNA levels of *CTGF* and *Cyr61* in MDA-MB-231, MDA-MB-436, and MCF-7 cells (Fig. 5b–c). These results suggested that PSVII reduced YAP expression and nuclear localization. To further investigate the role of YAP in PSVII-induced autophagy, BC cells overexpressing the YAP (YAP^{OE}) plasmid were generated after transient transfection. Interestingly, YAP^{OE} downregulated the PSVII-induced upregulation of LC3-II (Fig. 5d) and decreased the PSVII-induced accumulation of autophagosomes (Fig. 5f), suggesting that PSVII induced autophagy by downregulating YAP in BC cells. Furthermore, YAP^{OE} antagonized the PSVII-induced inhibition of cell proliferation and activation of apoptosis (Fig. 5e, g).

The upstream signal of YAP was further investigated, and Western blot analysis suggested that PSVII significantly increased the phosphorylation levels of LATS1 (pLATS1) and MOB1 (pMOB1) in MDA-MB-231, MDA-MB-436, and MCF-7 cells but had little effect on their total protein levels (Fig. 5h). MST1/2 phosphorylates and activates the LATS1/2-MOB1 complex. Next, the expression and phosphorylation of MST1/2 were investigated, and the results indicated that PSVII had little effect on the expression and phosphorylation of MST1/2 (Fig. 5h). These results suggest that PSVII may activate YAP-mediated autophagy by promoting the phosphorylation of LATS1 and MOB1.

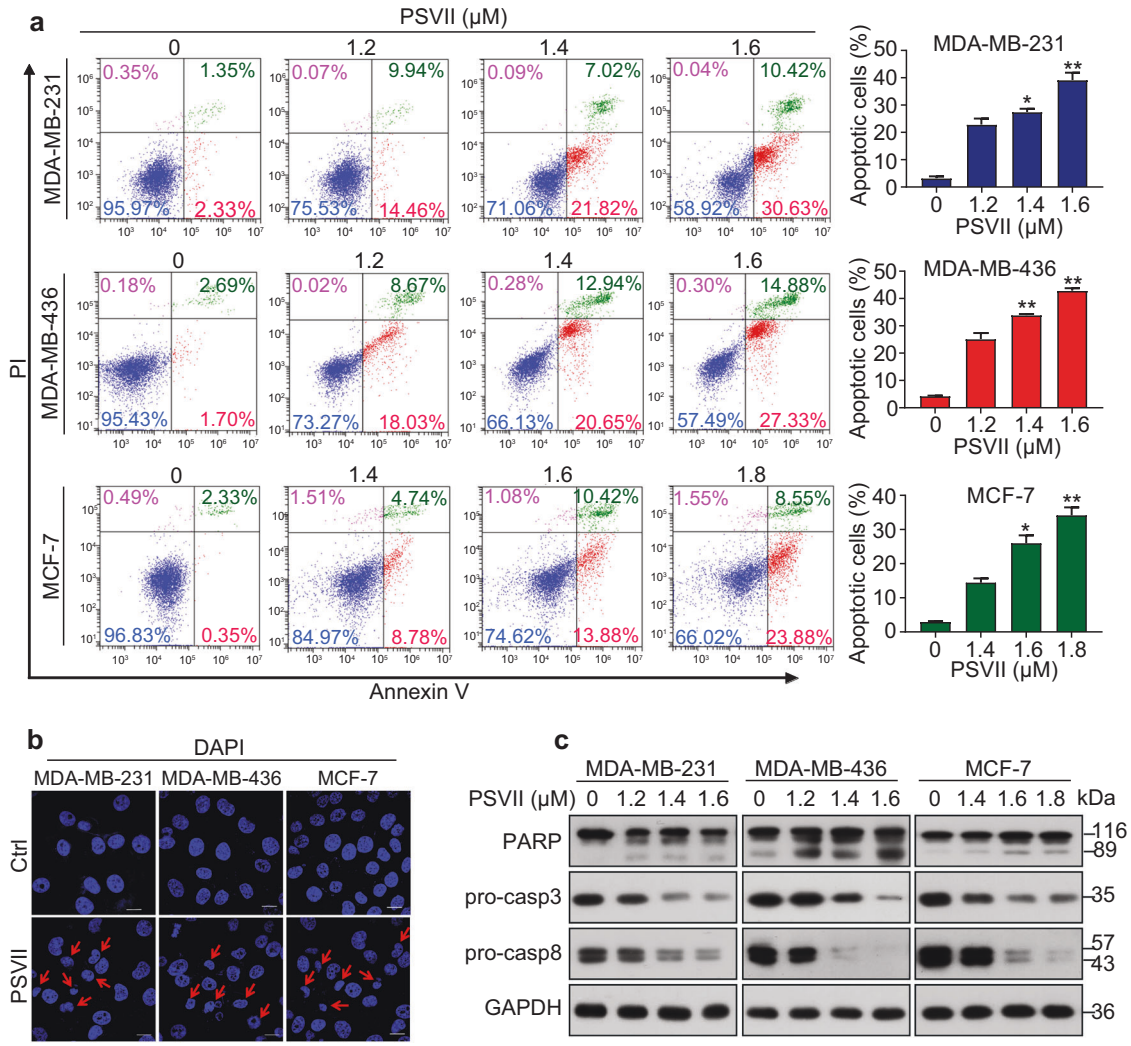

Fig. 3 PSVII induces the apoptosis of BC cells. a MDA-MB-231, MDA-MB-436, and MCF-7 cells were treated with PSVII for 24 h, and the cell apoptosis rate was assessed by annexin V/PI staining and flow cytometry. **b** MDA-MB-231, MDA-MB-436, and MCF-7 cells were incubated with or without PSVII (1.8 μM) for 24 h. The cells were examined by DAPI staining. **c** MDA-MB-231, MDA-MB-436, and MCF-7 cells were treated with increasing concentrations of PSVII for 24 h. Western blot was performed using the indicated antibodies. GAPDH was used as the loading control. $^{*}P < 0.05$, $^{**}P < 0.01$ compared with 0 μM. The data are representative of at least three experiments.

PSVII directly binds to the MST2-MOB1-LATS1 ternary complex to activate LATS1

LATS1 activation requires participation of all partners in the phosphorylation process. Multistep MST2-dependent phosphorylation and interaction involves MST2 itself, MOB1 and LATS1 [35]. Next, we sought to determine whether PSVII regulated the interaction of MST2/MOB1/LATS1. For this purpose, MDA-MB-231, MDA-MB-436, and MCF-7 cells were cotransfected with Myc-LATS1 and Flag-MST2 (or Myc-LATS1/HA-MOB1, Flag-MST2/HA-MOB1), and then treated with PSVII. Immunoprecipitation experiments demonstrated that in the presence of PSVII, the MST2/LATS1, MOB1/LATS1, and MST2/MOB1 interaction was dramatically enhanced (Fig. 6a–c). These results indicated that PSVII promoted the binding of MST2, MOB1 and LATS1, thereby promoting MOB1-mediated phosphorylation of LATS1.

The interaction of PSVII and Hippo signaling molecules was further determined in silico. Molecular docking experiments showed the interaction of PSVII with the crystal structure of the MST2-MOB1-LATS1 ternary complex (Fig. 6d). PSVII bound to the ternary complex with a binding energy of −5.08 kcal/mol (Fig. 6e) and interacted with a cluster of residues in each domain: Tyr396$_{(MST2)}$, Phe397$_{(MST2)}$, Glu176$_{(MOB1)}$, Ala177$_{(MOB1)}$, Asn180$_{(MOB1)}$, Thr181$_{(MOB1)}$, Lys184$_{(MOB1)}$, Val647$_{(LATS1)}$, Leu651$_{(LATS1)}$, and Gln655$_{(LATS1)}$ (Fig. 6f). Notably, the hydrogen atom on the six-membered ring of PSVII formed two hydrogen bonds with Phe397$_{(MST2)}$; the hydrogen bond lengths were 1.9 Å and 2.3 Å. The hydrogen atom on the six-membered ring of PSVII also formed four hydrogen bonds with Ala177$_{(MOB1)}$, Asn180$_{(MOB1)}$, and Thr181$_{(MOB1)}$; the bond lengths of these hydrogen bonds were 1.9 Å, 2.5 Å, 2.4 Å, and 2.3 Å (Fig. 6f). The formation of these hydrogen bonds enhanced the binding of PSVII to MST2 and MOB1 proteins and promoted the activation of LATS1. Next, microscale thermophoresis (MST) and drug affinity responsive targeting stability (DARTS) assays were performed to further detect the PSVII/MST2-MOB1-LATS1 interaction. Through MST, the equilibrium dissociation constant (K_d) value of PSVII and LATS1 was found to be 0.80 ± 0.37 mM, and the signal-to-noise ratio (S/N) was 43.3 (Fig. 6g). The K_d value of PSVII and MOB1 was 1.36 ± 0.46 mM, and the S/N was 48.1 (Fig. 6h). The K_d value of PSVII and MST2 was 0.42 ± 0.08 mM, and the S/N was 34.7 (Fig. 6i). These results indicated a strong binding affinity of PSVII and MST2-MOB1-LATS1. Furthermore, the DARTS assay is based on the idea that drug-target engagement

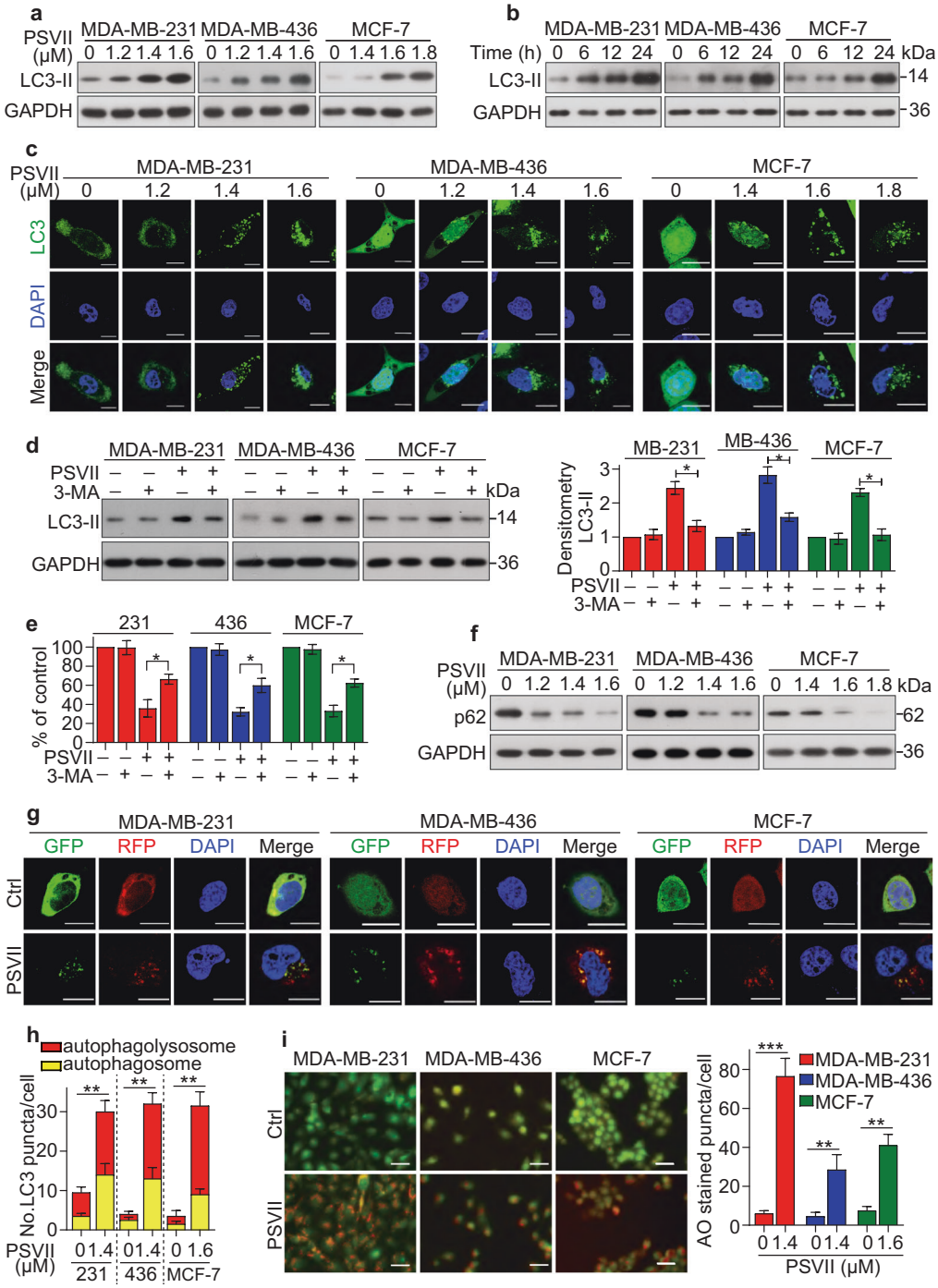

Fig. 4 PSVII induces autophagosome formation and promotes autophagic flux in BC cells. a MDA-MB-231, MDA-MB-436, and MCF-7 cells were treated with increasing concentrations of PSVII for 24 h. Western blot was performed using the indicated antibodies. **b** MDA-MB-231, MDA-MB-436, and MCF-7 cells were treated with PSVII (MDA-MB-231 cells, 1.4 μM; MDA-MB-436 cells, 1.4 μM; and MCF-7 cells, 1.6 μM) for the indicated times. Western blot was performed using the indicated antibodies. **c** MDA-MB-231, MDA-MB-436, and MCF-7 cells were transfected with the pQCXIP-GFP-LC3 plasmid for 6 h, treated with PSVII for another 24 h and assessed by immunofluorescence analysis. Scale bar = 15 μm. **d** MDA-MB-231, MDA-MB-436, and MCF-7 cells were treated with PSVII (MDA-MB-231 cells, 1.4 μM; MDA-MB-436 cells, 1.4 μM; and MCF-7 cells, 1.6 μM) and/or 3-MA (1 mM) for 24 h and analyzed by Western blot. **e** MDA-MB-231, MDA-MB-436, and MCF-7 cells were treated with PSVII (MDA-MB-231 cells, 1.4 μM; MDA-MB-436 cells, 1.4 μM; and MCF-7 cells, 1.6 μM) and/or 3-MA (1 mM) for 24 h and analyzed by CCK-8 assay. **f** MDA-MB-231 MDA-MB-436, and MCF-7 cells were treated with increasing concentrations of PSVII for 24 h. Western blot was performed using the indicated antibodies. **g, h** MDA-MB-231 MDA-MB-436, and MCF-7 cells were transfected with pmRFP-GFP-LC3 for 6 h and treated with PSVII (MDA-MB-231 cells, 1.4 μM; MDA-MB-436 cells, 1.4 μM; and MCF-7 cells, 1.6 μM) for another 24 h. The formation of autophagosomes (mRFP-positive; GFP-positive) and autophagolysosomes (mRFP-positive; GFP-negative) was examined and quantified by ImageJ software. Scale bar = 15 μm. **i** MDA-MB-231, MDA-MB-436, and MCF-7 cells were treated with PSVII (MDA-MB-231 cells, 1.4 μM; MDA-MB-436 cells, 1.4 μM; and MCF-7 cells, 1.6 μM) followed by acridine orange (AO) staining. Scale bar = 50 μm. Bar graph showed AO puncta per cell. *$P < 0.05$, **$P < 0.01$, ***$P < 0.001$.

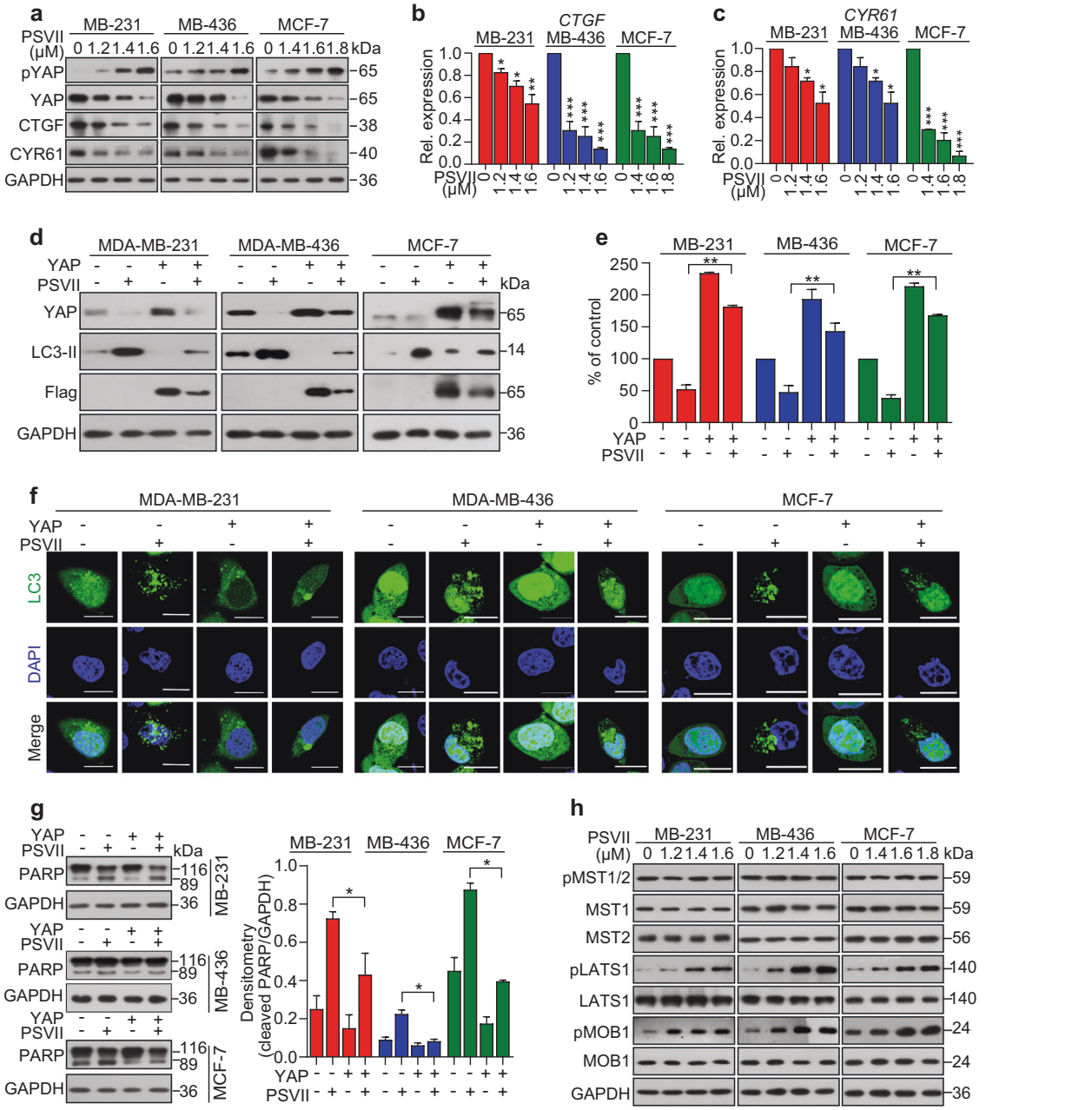

Fig. 5 PSVII induces autophagy via Hippo signaling pathway activation in BC cells. a MDA-MB-231, MDA-MB-436, or MCF-7 cells were treated with increasing concentrations of PSVII for 24 h. Western blot was performed using the indicated antibodies. **b**, **c** MDA-MB-231, MDA-MB-436, or MCF-7 cells were treated with increasing concentrations of PSVII for 24 h. The expression of *CTGF* or *Cyr61* was analyzed by qPCR. **d** MDA-MB-231, MDA-MB-436, or MCF-7 cells were transfected with the Flag-YAP plasmid for 24 h, then treated with PSVII (MDA-MB-231 cells, 1.4 μM; MDA-MB-436 cells, 1.4 μM; and MCF-7 cells, 1.6 μM) for another 24 h and assessed by Western blot analysis. **e** MDA-MB-231, MDA-MB-436, or MCF-7 cells were transfected with the Flag-YAP plasmid for 24 h, then treated with PSVII (MDA-MB-231 cells, 1.4 μM; MDA-MB-436 cells, 1.4 μM; and MCF-7 cells, 1.6 μM) for another 24 h and assessed by CCK-8 assay. **f** MDA-MB-231, MDA-MB-436, or MCF-7 cells were transfected with the Flag-YAP plasmid for 24 h, then treated with PSVII (MDA-MB-231 cells, 1.4 μM; MDA-MB-436 cells, 1.4 μM; and MCF-7 cells, 1.6 μM) for another 24 h and assessed by immunofluorescence analysis. **g** MDA-MB-231, MDA-MB-436, or MCF-7 cells were transfected with the Flag-YAP plasmid for 24 h, then treated with PSVII (MDA-MB-231 cells, 1.4 μM; MDA-MB-436 cells, 1.4 μM; and MCF-7 cells, 1.6 μM) for another 24 h and assessed by Western blot analysis. **h** MDA-MB-231, MDA-MB-436, or MCF-7 cells were treated with increasing concentrations of PSVII for 24 h. Western blot was performed using the indicated antibodies. *$P < 0.05$, **$P < 0.01$, ***$P < 0.001$.

protects against proteolysis of the target protein. As shown in Fig. 6j, PSVII significantly prevented the pronase-induced proteolysis of LATS1, MOB1, and MST2. These results demonstrated that PSVII directly binds to LATS1, MOB1, and MST2.

Overall, we conclude that PSVII induced autophagy and exhibited therapeutic potential in BC through directly activating of the Hippo pathway (Fig. 7).

PSVII inhibits tumor growth in murine models and shows a favorable pharmacokinetic profile

To determine the antitumor effect of PSVII on BC in vivo, MDA-MB-231 xenograft murine models were generated. Once the tumors grew to a measurable size, each group was administered vehicle ($n = 8$) or PSVII ($n = 8$) by i.p. injection at 1.5 mg/kg four times per week for 4 weeks (Fig. 8a). The tumor-bearing mice were

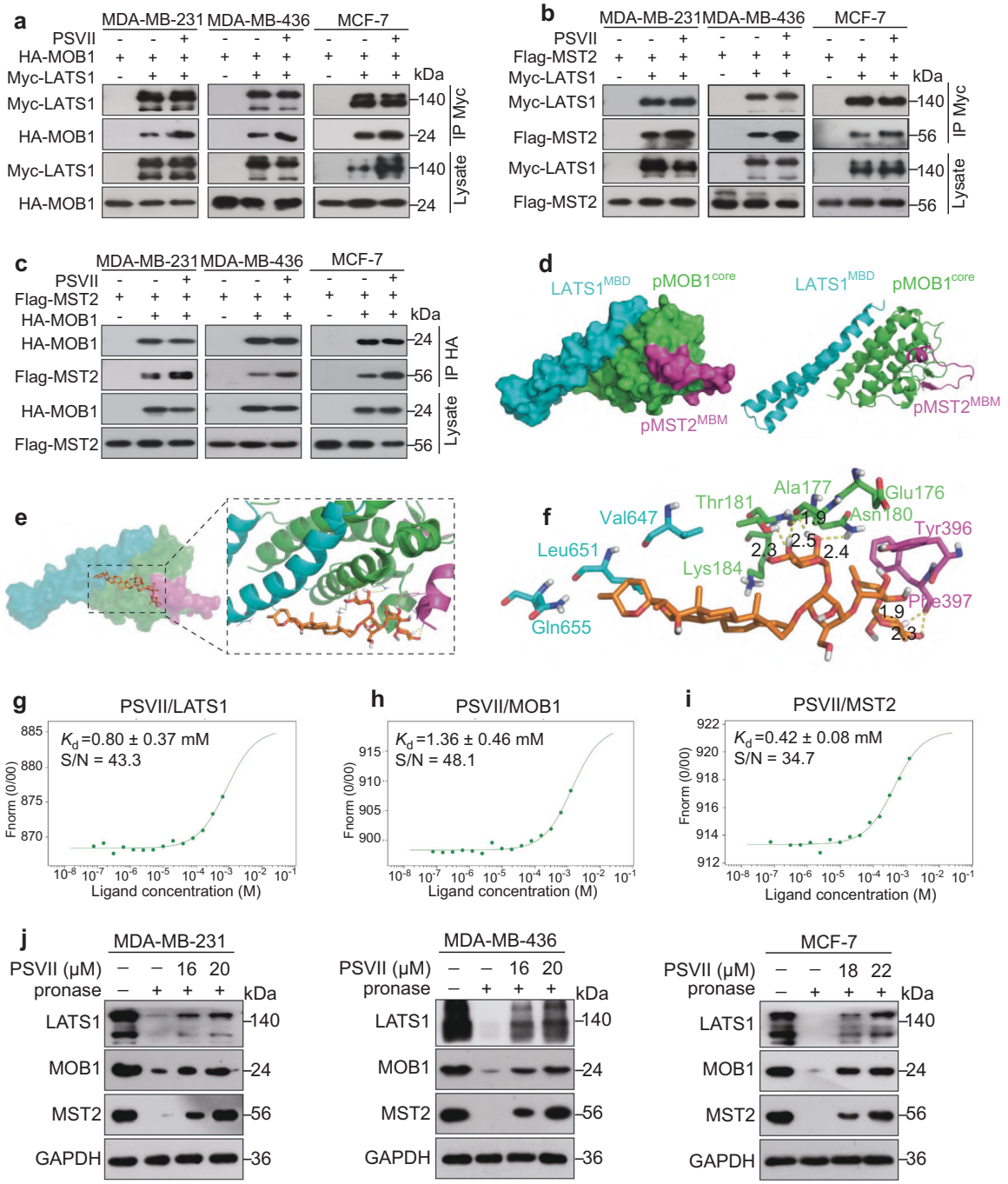

Fig. 6 PSVII directly binds to the MST2-MOB1-LATS1 ternary complex to activate LATS1. a MDA-MB-231, MDA-MB-436, or MCF-7 cells were cotransfected with the Myc-LATS1 and HA-MOB1 constructs for 24 h, followed by PSVII (MDA-MB-231 cells, 1.4 μM; MDA-MB-436 cells, 1.4 μM; and MCF-7 cells, 1.6 μM) treatment for 24 h, lysed, and the lysates were immunoprecipitated as indicated. **b** MDA-MB-231, MDA-MB-436, or MCF-7 cells were cotransfected with the Myc-LATS1 and Flag-MST2 constructs for 24 h, followed by PSVII (MDA-MB-231 cells, 1.4 μM; MDA-MB-436 cells, 1.4 μM; and MCF-7 cells, 1.6 μM) treatment for 24 h, lysed, and the lysates were immunoprecipitated as indicated. **c** MDA-MB-231, MDA-MB-436, or MCF-7 cells were cotransfected with the Myc-LATS1 and Flag-MST2 constructs for 24 h, followed by PSVII (MDA-MB-231 cells, 1.4 μM; MDA-MB-436 cells, 1.4 μM; and MCF-7 cells, 1.6 μM) treatment for 24 h, lysed, and the lysates were immunoprecipitated as indicated. **d** The protein surface and cartoon of the binding structure of the pMST2-pMOB1-LATS1 ternary complex. **e**, **f** The binding mode of PSVII docked into the pMST2-pMOB1-LATS1 ternary complex. The MOB1 binding domain of LATS1 ($LATS1^{MBD}$) is cyan, the core of MOB1 ($MOB1^{core}$) is green, the MOB1 binding motif of MST2 ($MST2^{MBM}$) is magenta and PSVII is gold. **g**–**i** Binding affinity of PSVII with LATS1, MOB1, and MST2 by MST assay in standard treated capillaries. **j** MDA-MB-231, MDA-MB-436, or MCF-7 cell lysates were incubated in the presence or absence of PSVII for 30 min at room temperature, followed by proteolysis with pronase. GAPDH, which served as the loading control, was relatively resistant to proteolysis. The data are representative of at least three experiments.

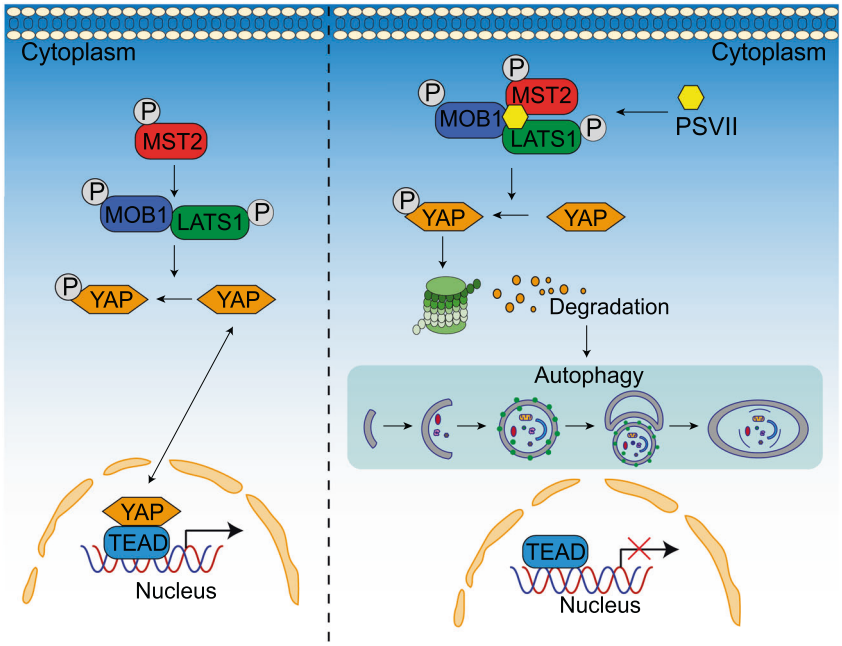

Fig. 7 Schematic representation of the mechanism of action of PSVII. PSVII binds the pMST2-pMOB1-LATS1 ternary complex, thereby promoting YAP degradation, leading to BC cell autophagy.

euthanized when their tumors reached 1.5 cm in diameter, when they were paralyzed or when their quality of life was otherwise compromised. The results showed that PSVII efficiently suppressed tumor growth compared with the vehicle control (Fig. 8b–c). PSVII treatment also significantly reduced the tumor weight of the mice (Fig. 8d). In addition, PSVII treatment did not significantly reduce the body weight of the mice (Fig. 8e). The mice were euthanized, and the tumor specimens were examined by Western blot analysis and immunohistochemistry. The results showed that in the PSVII-treated groups, the expression levels of pLATS1, LC3-II, and Beclin 1 were upregulated, and those of YAP, p62, and Ki67 were downregulated (Fig. 8f–g).

The pharmacokinetic features of PSVII were then tested in SD rats. To this end, four rats were administered PSVII (1 mg/kg) by intravenous (i.v.) injection, and another four rats were inoculated with PSVII (10 mg/kg) by intragastric (i.g.) injection. The mean plasma concentration-time profiles are shown in Fig. 8h and i, and the main pharmacokinetic parameters are summarized in Table 3. The results indicated that in the four rats that received an i.v. injection of 1 mg/kg PSVII, the plasma PSVII level reached a peak concentration of 2.993 ± 0.715 mg/L within 0.074 h with a $t_{1/2}$ of 3.185 h. In four rats administered 10 mg/kg PSVII via i.g. injection, plasma PSVII level reached a peak concentration of 0.402 ± 0.136 mg/L at 1.350 h with a $t_{1/2}$ of 3.722 h. These results demonstrated that the administration of PSVII via i.v. injection reached the therapeutic concentration of PSVII in vivo.

DISCUSSION

It has been reported that steroidal saponins exert significant cytotoxicity in several tumor types [36, 37]. The key to the antitumor effects of these drugs is the common steroid nucleus. In previous studies, we found that the toxic effects of polyphyllin I and PSVII on the same lung cancer cell line were not much different [38, 39]. Yin et al. used a rapid and specific LC-MS-MS method to analysis the pharmacokinetics of polyphyllin I, polyphyllin II, polyphyllin VI, and PSVII in beagle dog plasma and found that Polyphyllin I showed a higher maximum observed plasma concentration and a longer mean residence time [40]. Here, our data established PSVII as a novel activator of the Hippo signaling pathway, which induced cytotoxic autophagy in BC cells.

Apoptosis is the main mechanism by which many chemotherapeutics kill tumor cells. One of the main mechanisms by which PSVII reduces cell viability may be through the induction of cell apoptosis, which was first shown by the increase in Annexin V^+/PI^- cells and cell morphological characteristics indicative of apoptosis. In addition, as the main initiator of the external apoptotic pathway [41], pro-casp8 was reduced at the protein level by PSVII treatment, which suggests that the external apoptotic pathway is related to PSVII-induced apoptosis.

Shen and Codogno [42] proposed that autophagic cell death be defined as a mode of nonapoptotic or necrotic programmed cell death; that is, autophagy as a cell death mechanism meets the following three criteria: (i) cell death occurs without apoptosis; (ii) autophagic flux increases in the dying cells, with an increase in autophagy markers; and (iii) inhibition of autophagy through pharmacological inhibitors or genetic methods prevents cell death. Nevertheless, in many cases, autophagy and apoptosis are used as parallel pathways to promote cell death. For instance, Feng et al. [43] recently showed that tubeimoside I inhibited cervical cancer cells by both initiating autophagy and inducing apoptosis. Liu et al. [44] also showed that apatinib promotes autophagy and apoptosis through VEGFR2/STAT3/BCL-2 signaling in osteosarcoma. The current study demonstrated that PSVII induced the biosynthesis of autophagosomes, which are subsequently engulfed by lysosomes to form autophagolysosomes. PSVII promotes the process of autophagic flux. These data suggest that PSVII functions as a promising antitumor agent by both initiating autophagy and inducing apoptosis.

Emerging evidence suggests that the cross talk between Hippo signaling pathway components and autophagy impacts physiology and cancer progression [45]. On the one hand, autophagy regulates Hippo signaling activity. Under conditions of starvation or therapeutic stress, AMPK and ULK1, the key signaling molecules upstream of autophagy, inactivate YAP through direct phosphorylation or indirect regulation, thereby inhibiting YAP-driven

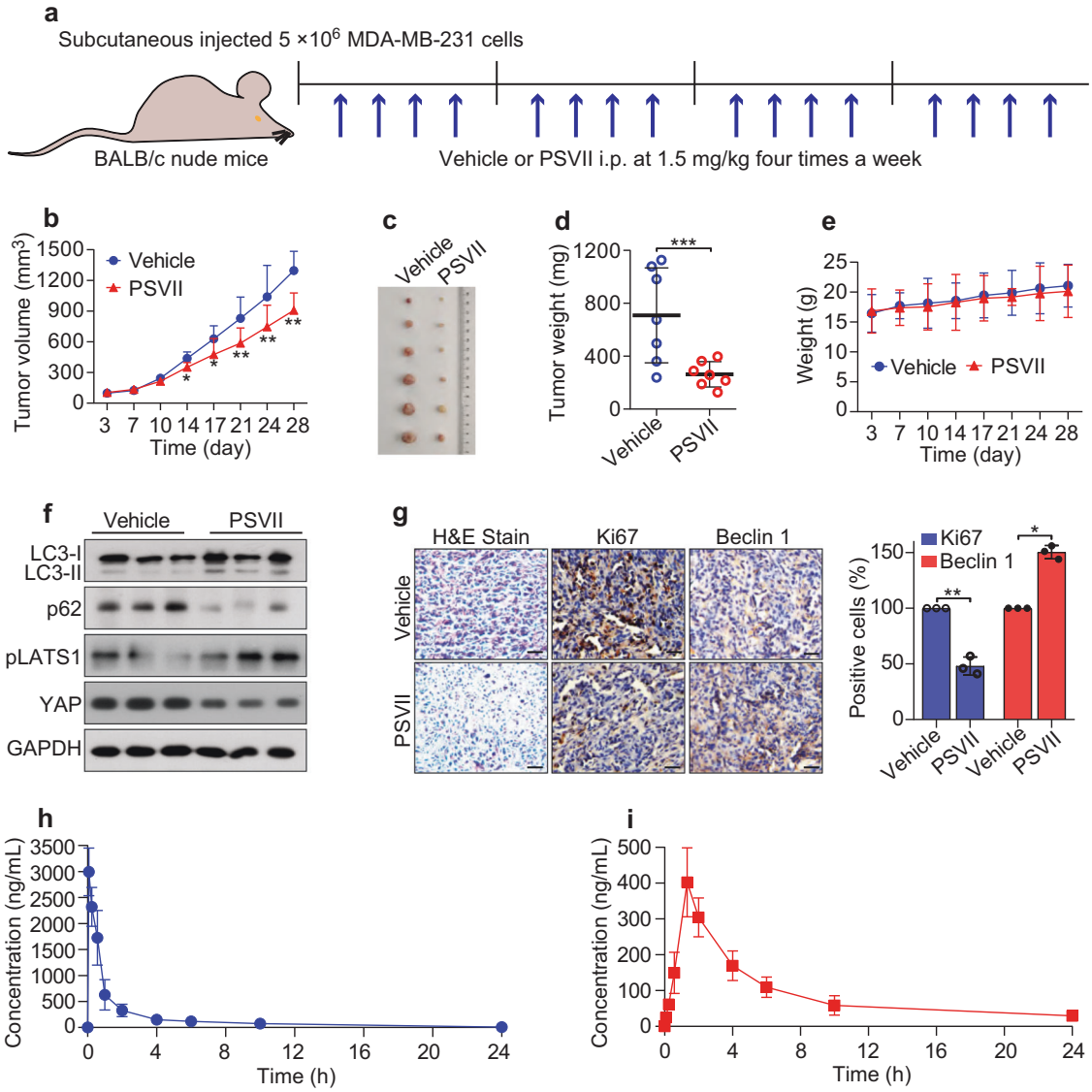

Fig. 8 PSVII inhibits tumor growth in murine models and shows favorable pharmacokinetic profiles. a Process diagram of xenograft tumor models. **b** Murine models were treated with vehicle or 1.5 mg/kg PSVII and the tumor volumes were calculated twice a week. **c** Images of xenograft tumors obtained from mice subjected to different treatments after 4 weeks. **d** Weight of the tumor from each group removed from the sacrificed mice at the end of the study. **e** PSVII treatment did not affect the murine model body weight. **f** The expression of the indicated protein in xenograft tumors was analyzed by Western blot. **g** Representative tumor tissues were sectioned and subjected to H&E staining, and immunohistochemistry staining for Ki67 and Beclin1. Scale bar = 50 μm. **h** The concentration-time profiles of PSVII after i.v. injection (1 mg/kg) in SD rats. **i** The concentration-time profiles of PSVII after i.g. injection (10 mg/kg) in SD rats. $^{*}P < 0.05$, $^{**}P < 0.01$, $^{***}P < 0.001$ vs vehicle.

Table 3. Pharmacokinetic parameters of PSVII in SD rats.

Administration and dosage	$T_{1/2}$ (h)	$AUC_{0\text{-}t}$ (mg/L·h)	T_{max} (h)	C_{max} (mg/L)	$MRT_{0\text{-}t}$ (h)	CL_z ($L \cdot h^{-1} \cdot kg^{-1}$)	BA (%)
i.v. (1 mg/kg)	3.185 ± 0.964	2.961 ± 0.983	0.074 ± 0.000	2.993 ± 0.715	1.956 ± 0.423	0.435 ± 0.086	—
i.g. (10 mg/kg)	3.722 ± 1.257	2.476 ± 1.048	1.35 ± 0.000	0.402 ± 0.136	5.491 ± 1.286	4.127 ± 0.389	13.86

AUC Area under the plasma concentration time curve, *BA* bioavailability, *CL* total plasma clearance, C_{max} maximum observed plasma concentration, *i.v.* intravenous injection, *i.g.* intragastric injection, *MRT* mean residence time, $T_{1/2}$ terminal elimination phase half-life.

carcinogenic events [46, 47]. On the other hand, Hippo signaling mediates autophagy regulation. The YAP/TAZ/TEAD transcription complex promotes autophagosome maturation and autophagy [48]. LATS1/2 and MST1/2 kinase also directly phosphorylate LC3B and BECN1 to regulate autophagy [49, 50]. This study found that PSVII downregulated the expression of YAP and its downstream target genes by promoting its phosphorylation. Furthermore, PSVII significantly upregulated the activity of LATS1 and MOB1. The formation of the MST2-MOB1-LATS1 ternary complex promoted the phosphorylation cascade of MOB1 and LATS1 by MST2 [35]. Immunoprecipitation experiments proved that PSVII promoted the binding of LATS1 to MST2 and MOB1, which is a prerequisite for

increased phosphorylation of LATS1. Molecular docking experiments revealed that PSVII tightly binds to the crystal structure of the MST2-MOB1-LATS1 ternary complex. PSVII formed six hydrogen bonds with $Phe397_{(MST2)}$, $Ala177_{(MOB1)}$, $Asn180_{(MOB1)}$, and $Thr181_{(MOB1)}$ on MST2 and MOB1, respectively. Next, we performed MST assay to confirm the in silico prediction. MST assay is a highly sensitive biochemical method for measuring interactions. It is based on the movement of a given protein along a temperature gradient (thermophoresis) to characterize the interaction between a ligand and the receptor [51]. PSVII exhibited binding affinity for LATS1, MOB1, and MST2, with K_d values of 0.80 ± 0.37, 1.36 ± 0.46, and 0.42 ± 0.08 mM, respectively. DARTS is a method used to identify the target proteins of small molecules without chemical modification [52]. This method confirmed the interaction between PSVII and MST2, MOB1, and LATS1 in BC cells. Together with MST2, MOB1, and LATS1, PSVII forms a stable conformation to constitutively activate LATS1.

In summary, this study analyzed a natural compound, PSVII, which directly binds to the MST2-MOB1-LATS1 ternary complex and activates LATS1 and MOB1, exhibiting an anticancer effect on BC cells. PSVII induces autophagy and apoptosis to inhibit cancer cell proliferation. According to our results, PSVII is a potential and promising agent to treat BC patients by activating autophagy. In addition, it can potentially be used as a beneficial drug tool for Hippo pathway research.

ACKNOWLEDGEMENTS

This work was supported by grants from the National Natural Science Foundation of China (Nos 82072928 and 81802387), the Foundation for Innovative Research Group of Hubei Provincial Department of Science and Technology (No. 2021CFA071), the Foundation for Innovative Research Team of Hubei Provincial Department of Education (No. T201915), the Principal Investigator Grant of Hubei University of Medicine (No. HBMUPI201806), the Innovative Research Program for Graduates (No. YC2021004), the Faculty Development Grants from Hubei University of Medicine (No. 2018QDJZR03), the Scientific and Technological Project of Shiyan City of Hubei Province (Nos 21Y08 and 21Y09), and the National Training Program of Innovation and Entrepreneurship for Undergraduates (Nos 202110929001 and 202110929002).

AUTHOR CONTRIBUTIONS

YL conceived and planned the experiments. YCX, PP, XWL, XJ, JS, TZ, LZ, FW, YLR, QQY, and HZZ performed the experiment and analyzed the data. YL and YS wrote the paper.

ADDITIONAL INFORMATION

Supplementary information The online version contains supplementary material available at https://doi.org/10.1038/s41401-021-00755-9.

Competing interests: The authors declare no competing interests.

REFERENCES

1. Sung H, Ferlay J, Siegel RL, Laversanne M, Soerjomataram I, Jemal A, et al. Global cancer statistics 2020: GLOBOCAN estimates of incidence and mortality worldwide for 36 cancers in 185 countries. CA Cancer J Clin. 2021;71:209–49.
2. Zeng H, Chen W, Zheng R, Zhang S, Ji JS, Zou X, et al. Changing cancer survival in China during 2003-15: a pooled analysis of 17 population-based cancer registries. Lancet Glob Health. 2018;6:e555–e67.
3. Ehsan H, Imtiaz H, Sana MK, Sheikh MM, Wahab A. Relapsed breast cancer complicated by isolated brain metastasis. Clin Case Rep. 2021;9:887–90.
4. Levy JMM, Towers CG, Thorburn A. Targeting autophagy in cancer. Nat Rev Cancer. 2017;17:528–42.
5. Cao W, Li J, Yang K, Cao D. An overview of autophagy: mechanism, regulation and research progress. Bull Cancer. 2021;108:304–22.
6. Limpert AS, Lambert LJ, Bakas NA, Bata N, Brun SN, Shaw RJ, et al. Autophagy in cancer: regulation by small molecules. Trends Pharmacol Sci. 2018;39:1021–32.
7. Russo M, Russo GL. Autophagy inducers in cancer. Biochem Pharmacol. 2018; 153:51–61.
8. Takahashi A, Kimura F, Yamanaka A, Takebayashi A, Kita N, Takahashi K, et al. Metformin impairs growth of endometrial cancer cells via cell cycle arrest and concomitant autophagy and apoptosis. Cancer Cell Int. 2014;14:53.
9. Fu H, Wang C, Yang D, Wei Z, Xu J, Hu Z, et al. Curcumin regulates proliferation, autophagy, and apoptosis in gastric cancer cells by affecting PI3K and P53 signaling. J Cell Physiol. 2018;233:4634–42.
10. Bi Y, Shen C, Li C, Liu Y, Gao D, Shi C, et al. Inhibition of autophagy induced by quercetin at a late stage enhances cytotoxic effects on glioma cells. Tumour Biol. 2016;37:3549–60.
11. Si Y, Ji X, Cao X, Dai X, Xu L, Zhao H, et al. Src inhibits the Hippo tumor suppressor pathway through tyrosine phosphorylation of Lats1. Cancer Res. 2017;77:4868–80.
12. Han Y. Analysis of the role of the Hippo pathway in cancer. J Transl Med. 2019;17:116.
13. Dey A, Varelas X, Guan KL. Targeting the Hippo pathway in cancer, fibrosis, wound healing and regenerative medicine. Nat Rev Drug Discov. 2020;19:480–94.
14. Cao J, Huang W. Two faces of Hippo: activate or suppress the Hippo pathway in cancer. Anticancer Drugs. 2017;28:1079–85.
15. Zheng Y, Pan D. The Hippo signaling pathway in development and disease. Dev Cell. 2019;50:264–82.
16. Calses PC, Crawford JJ, Lill JR, Dey A. Hippo pathway in cancer: aberrant regulation and therapeutic opportunities. Trends Cancer. 2019;5:297–307.
17. Wu L, Yang X. Targeting the Hippo pathway for breast cancer therapy. Cancers (Basel). 2018;10:422.
18. Wang BL, Zhang H, Hao XC, Ge ZK, Qiu JR, Zhao YH. Research progress on pharmacological action of *Trillium tschonoskii* Maxim. J Tradit Chin Med. 2018;40: 478–81.
19. Wang BL, Hao XC, Ge ZK, Qiu JR, Zhang H, Zhao YH. Study on HPLC fingerprint of *Trillium tschonoskii* Maxim. Hubei J Tradit Chin Med. 2018;37:225–8.
20. Lin X, Gajendran B, Varier KM, Liu W, Song J, Rao Q, et al. Paris Saponin VII induces apoptosis and cell cycle arrest in erythroleukemia cells by a mitochondrial membrane signaling pathway. Anticancer Agents Med Chem. 2020;21:498–507.
21. Tang GE, Niu YX, Li Y, Wu CY, Wang XY, Zhang J. Paris saponin VII enhanced the sensitivity of HepG2/ADR cells to ADR via modulation of PI3K/AKT/MAPK signaling pathway. Kaohsiung J Med Sci. 2020;36:98–106.
22. Li Y, Sun Y, Fan L, Zhang F, Meng J, Han J, et al. Paris saponin VII inhibits growth of colorectal cancer cells through Ras signaling pathway. Biochem Pharmacol. 2014;88:150–7.
23. Zhang W, Zhang D, Ma X, Liu Z, Li F, Wu D. Paris saponin VII suppressed the growth of human cervical cancer Hela cells. Eur J Med Res. 2014;19:41.
24. Fan L, Li Y, Sun Y, Han J, Yue Z, Meng J, et al. Paris saponin VII inhibits the migration and invasion in human A549 lung cancer cells. Phytother Res. 2015; 29:1366–72.
25. Cheng G, Gao F, Sun X, Bi H, Zhu Y. Paris saponin VII suppresses osteosarcoma cell migration and invasion by inhibiting MMP2/9 production via the p38 MAPK signaling pathway. Mol Med Rep. 2016;14:3199–205.
26. Zhang Y, Huang P, Liu X, Xiang Y, Zhang T, Wu Y, et al. Polyphyllin I inhibits growth and invasion of cisplatin-resistant gastric cancer cells by partially inhibiting CIP2A/PP2A/Akt signaling axis. J Pharm Sci. 2018;137:305–12.
27. Ma WJ, Xiang YC, Yang R, Zhang T, Xu JX, Wu YZ, et al. Cucurbitacin B induces inhibitory effects via the CIP2A/PP2A/C-KIT signaling axis in t(8;21) acute myeloid leukemia. J Pharm Sci. 2019;139:304–10.
28. Liu PF, Xiang YC, Liu XW, Zhang T, Yang R, Chen S, et al. Cucurbitacin B induces the lysosomal degradation of EGFR and suppresses the CIP2A/PP2A/Akt signaling axis in gefitinib-resistant non-small cell lung cancer. Molecules. 2019;24:647.
29. Si Y, Wang J, Liu X, Zhou T, Xiang Y, Zhang T, et al. Ethoxysanguinarine, a novel direct activator of AMP-activated protein kinase, induces autophagy and exhibits therapeutic potential in breast cancer cells. Front Pharmacol. 2019;10:1503.
30. Wang Q, Zhang Q, Luan S, Yang K, Zheng M, Li K, et al. Adapalene inhibits ovarian cancer ES-2 cells growth by targeting glutamic-oxaloacetic transaminase 1. Bioorg Chem. 2019;93:103315.
31. Choi J, Lee YJ, Yoon YJ, Kim CH, Park SJ, Kim SY, et al. Pimozide suppresses cancer cell migration and tumor metastasis through binding to ARPC2, a subunit of the Arp2/3 complex. Cancer Sci. 2019;110:3788–801.
32. Lee YK, Jun YW, Choi HE, Huh YH, Kaang BK, Jang DJ, et al. Development of LC3/GABARAP sensors containing a LIR and a hydrophobic domain to monitor autophagy. EMBO J. 2017;36:1100–16.
33. Bjorkoy G, Lamark T, Pankiv S, Overvatn A, Brech A, Johansen T. Monitoring autophagic degradation of p62/SQSTM1. Methods Enzymol. 2009;452:181–97.
34. Lv X, Li K, Hu Z. Autophagy and pulmonary fibrosis. Adv Exp Med Biol. 2020;1207: 569–79.
35. Ni L, Zheng Y, Hara M, Pan D, Luo X. Structural basis for Mob1-dependent activation of the core Mst-Lats kinase cascade in Hippo signaling. Genes Dev. 2015;29:1416–31.

36. Zhao YZ, Zhang YY, Han H, Fan RP, Hu Y, Zhong L, et al. Advances in the antitumor activities and mechanisms of action of steroidal saponins. Chin J Nat Med. 2018;16:732–48.
37. Man S, Gao W, Zhang Y, Huang L, Liu C. Chemical study and medical application of saponins as anti-cancer agents. Fitoterapia 2010;81:703–14.
38. Xiang YC, Shen J, Si Y, Liu XW, Zhang L, Wen J, et al. Paris saponin VII, a direct activator of AMPK, induces autophagy and exhibits therapeutic potential in non-small-cell lung cancer. Chin J Nat Med. 2021;19:195–204.
39. Wu Y, Si Y, Xiang Y, Zhou T, Liu X, Wu M, et al. Polyphyllin I activates AMPK to suppress the growth of non-small-cell lung cancer via induction of autophagy. Arch Biochem Biophys. 2020;687:108285.
40. Yin X, Qu C, Li Z, Zhai Y, Cao S, Lin L, et al. Simultaneous determination and pharmacokinetic study of polyphyllin I, polyphyllin II, polyphyllin VI and polyphyllin VII in beagle dog plasma after oral administration of Rhizoma Paridis extracts by LC-MS-MS. Biomed Chromatogr. 2013;27:343–8.
41. Tummers B, Green DR. Caspase-8: regulating life and death. Immunol Rev. 2017;277:76–89.
42. Shen HM, Codogno P. Autophagic cell death: Loch Ness monster or endangered species? Autophagy. 2011;7:457–65.
43. Feng X, Zhou J, Li J, Hou X, Li L, Chen Y, et al. Tubeimoside I induces accumulation of impaired autophagolysosome against cervical cancer cells by both initiating autophagy and inhibiting lysosomal function. Cell Death Dis. 2018;9:1117.
44. Liu K, Ren T, Huang Y, Sun K, Bao X, Wang S, et al. Apatinib promotes autophagy and apoptosis through VEGFR2/STAT3/BCL-2 signaling in osteosarcoma. Cell Death Dis. 2017;8:e3015.
45. Tang F, Christofori G. The cross-talk between the Hippo signaling pathway and autophagy:implications on physiology and cancer. Cell Cycle. 2020;19:2563–72.
46. Mo JS, Meng Z, Kim YC, Park HW, Hansen CG, Kim S, et al. Cellular energy stress induces AMPK-mediated regulation of YAP and the Hippo pathway. Nat Cell Biol. 2015;17:500–10.
47. Kim J, Kundu M, Viollet B, Guan KL. AMPK and mTOR regulate autophagy through direct phosphorylation of Ulk1. Nat Cell Biol. 2011;13:132–41.
48. Totaro A, Zhuang Q, Panciera T, Battilana G, Azzolin L, Brumana G, et al. Cell phenotypic plasticity requires autophagic flux driven by YAP/TAZ mechanotransduction. Proc Natl Acad Sci USA. 2019;116:17848–57.
49. Wilkinson DS, Jariwala JS, Anderson E, Mitra K, Meisenhelder J, Chang JT, et al. Phosphorylation of LC3 by the Hippo kinases STK3/STK4 is essential for autophagy. Mol Cell. 2015;57:55–68.
50. Gan W, Dai X, Dai X, Xie J, Yin S, Zhu J, et al. LATS suppresses mTORC1 activity to directly coordinate Hippo and mTORC1 pathways in growth control. Nat Cell Biol. 2020;22:246–56.
51. Wienken CJ, Baaske P, Rothbauer U, Braun D, Duhr S. Protein-binding assays in biological liquids using microscale thermophoresis. Nat Commun. 2010;1:100.
52. Chang J, Kim Y, Kwon HJ. Advances in identification and validation of protein targets of natural products without chemical modification. Nat Prod Rep. 2016;33:719–30.